

Preconditioning nonlocal multi-phase flow

David Kay

Department of Computer Science, University of Oxford, Oxford, OX1 3QD, UK

Vanessa Styles*

Department of Mathematics, University of Sussex, Brighton, BN1 9RF, UK

Abstract

We propose an efficient solver for saddle point problems arising from finite element approximations of nonlocal multi-phase Allen–Cahn variational inequalities. The solver is seen to behave mesh independently and to have only a very mild dependence on the number of phase field variables. In addition we prove convergence, in three GMRES iterations, of the approximation of the two phase problem, regardless of mesh size or interfacial width. Numerical results are presented that illustrate the competitiveness of this approach.

Keywords: Allen–Cahn systems; nonlocal constraints; PDE-constrained optimization; primal–dual active set method; saddle point systems; preconditioning; Krylov subspace solver

1. Introduction

s:intro

The aim of this paper is to combine preconditioning methods for indefinite problems and multigrid preconditioning developed for elliptic systems to provide an efficient preconditioner for the solution of systems of multiphase Allen–Cahn
5 variational inequalities of the form:

$\mathcal{P}_{\mathbf{Q}}$: For given $\mathbf{u}(\cdot, 0) = \mathbf{u}_0 \in \mathcal{G}_{\mathbf{Q}}$, find $\mathbf{u} \in L^2(0, T; \mathcal{G}_{\mathbf{Q}}) \cap H^1(0, T; \mathbf{L}^2(\Omega))$

*Corresponding author

Email address: `v.styles@sussex.ac.uk` (Vanessa Styles)

such that

$$\varepsilon \left(\frac{\partial \mathbf{u}}{\partial t}, \boldsymbol{\chi} - \mathbf{u} \right) + \varepsilon (\nabla \mathbf{u}, \nabla (\boldsymbol{\chi} - \mathbf{u})) - \frac{1}{\varepsilon} (\mathbf{A} \mathbf{u}, \boldsymbol{\chi} - \mathbf{u}) \geq 0, \forall \boldsymbol{\chi} \in \mathcal{G}_{\mathbf{Q}}.$$

Here $\Omega \in \mathbb{R}^d$, $d = 1, 2$ or 3 and $\mathbf{u} : \Omega \times (0, T) \rightarrow \mathbb{R}^N$ denotes the vector-valued phase field function which describes the fractions of the N phases, i.e. each component of \mathbf{u} describes one phase, $\mathbf{A} \in \mathbb{R}^{N \times N}$ is a symmetric constant matrix that has at least one positive eigenvalue,

$$\mathcal{G}_{\mathbf{Q}} := \{\mathbf{v} \in \mathbf{H}^1(\Omega) \mid \mathbf{v} \in G_{\mathbf{Q}} \text{ a.e.}\}$$

with

$$G_{\mathbf{Q}} := \{\boldsymbol{\xi} \in \mathbb{R}^N \mid \boldsymbol{\xi} \geq \mathbf{0}, \boldsymbol{\xi} \cdot \mathbf{1} = 1, \int_{\Omega} \mathbf{v} \, d\mathbf{x} = \mathbf{Q}\}.$$

We denote by $\mathbf{L}^2(\Omega)$ and $\mathbf{H}^1(\Omega)$ the spaces of vector-valued functions, (\cdot, \cdot) is the standard L^2 inner product for scalar functions, $(\mathbf{v}, \mathbf{w}) = \sum_{i=1}^N (v_i, w_i)$ for $\mathbf{v}, \mathbf{w} \in \mathbf{L}^2(\Omega)$, $(\mathbf{A}, \mathbf{B}) = \sum_{i=1}^N \sum_{j=1}^d (a_{ij}, b_{ij})$ for matrix-valued functions, $\boldsymbol{\xi} \geq \mathbf{0}$ means $\xi_i \geq 0$ for all $i \in \{1, \dots, N\}$, $\mathbf{1} = (1, \dots, 1)^T$, $\boldsymbol{\xi} \cdot \mathbf{1} = \sum_{i=1}^N \xi_i$ and $\int_{\Omega} f(x) \, d\mathbf{x} := \frac{1}{|\Omega|} \int_{\Omega} f(x) \, d\mathbf{x}$.

The system $\mathcal{P}_{\mathbf{Q}}$ arises from steepest descent dynamics with respect to the L^2 -norm of the Ginzburg-Landau energy,

$$E(\mathbf{u}) := \int_{\Omega} \left(\frac{\varepsilon}{2} |\nabla \mathbf{u}|^2 + \frac{1}{\varepsilon} \Psi(\mathbf{u}) \right) d\mathbf{x},$$

under the constraint $\int_{\Omega} \mathbf{u} \, d\mathbf{x} = \mathbf{Q}$. Here Ψ is the multi-obstacle potential

$$\Psi(\theta) := -\frac{1}{2} \theta^T \mathbf{A} \theta + I_G = \begin{cases} -\frac{1}{2} \theta^T \mathbf{A} \theta & \text{for } \theta \in \mathcal{G} \\ \infty & \text{otherwise} \end{cases}$$

with I_G denoting the indicator function for the Gibbs Simplex, $G := \{\boldsymbol{\xi} \in \mathbb{R}^N \mid \boldsymbol{\xi} \geq \mathbf{0}, \boldsymbol{\xi} \cdot \mathbf{1} = 1\}$, and the symmetric constant matrix \mathbf{A} has at least one positive eigenvalue to allow for minima of Ψ to exist, see [1].

Remark 1.1. *Steepest descent dynamics with respect to the L^2 -norm of the Ginzburg-Landau energy $E(\mathbf{u})$, without the constraint $\int_{\Omega} \mathbf{u} \, d\mathbf{x} = \mathbf{Q}$, yields the*

system:

\mathcal{P} : For given $\mathbf{u}(\cdot, 0) = \mathbf{u}_0 \in \mathcal{G}$, find $\mathbf{u} \in L^2(0, T; \mathcal{G}) \cap H^1(0, T; \mathbf{L}^2(\Omega))$ such that

$$\varepsilon \left(\frac{\partial \mathbf{u}}{\partial t}, \boldsymbol{\chi} - \mathbf{u} \right) + \varepsilon (\nabla \mathbf{u}, \nabla (\boldsymbol{\chi} - \mathbf{u})) - \frac{1}{\varepsilon} (\mathbf{A} \mathbf{u}, \boldsymbol{\chi} - \mathbf{u}) \geq 0, \quad \forall \boldsymbol{\chi} \in \mathcal{G}$$

where $\mathcal{G} := \{\mathbf{v} \in \mathbf{H}^1(\Omega) \mid \mathbf{v} \in G \text{ a.e.}\}$. Since \mathcal{P} is a simplified version of $\mathcal{P}_{\mathbf{Q}}$
 15 the solver we propose in this paper can be applied to the corresponding finite
 element approximation of \mathcal{P} .

\mathcal{P} is a generalisation of the scalar Allen–Cahn equation that was introduced
 by Allen and Cahn [2] to describe the capillarity driven evolution of an interface
 separating two bulk phases. The parameter ε , with $0 < \varepsilon \ll 1$, is associated with
 20 the thickness of the diffuse interfacial layer in which the phase field variables
 rapidly change their value. The N phase extension of the scalar Allen–Cahn
 model was introduced in [3, 4]. The nonlocal problem $\mathcal{P}_{\mathbf{Q}}$ models interface
 evolution with mass conservation.

Multiphase Allen–Cahn models have a variety of applications, including im-
 25 age segmentation, see for example [5], and identification of coefficients in elliptic
 equations [7]. Applications arising from identification of coefficients in elliptic
 equations include electric impedance tomography, [8, 9, 10], and flow in porous
 media with unknown permeabilities [11, 12, 13]. Applications of mass conserving
 multiphase Allen–Cahn models include structural topology optimisation [14, 15].

Efficient and reliable, i.e., fast and globally converging, multigrid methods
 30 for solving implicit in time finite element approximations of \mathcal{P} are presented
 in [16, 17], while an explicit in time finite element approximation of $\mathcal{P}_{\mathbf{Q}}$ was
 introduced in [18]. In [19] (semi-)implicit in time finite element approximations
 of $\mathcal{P}_{\mathbf{Q}}$ are considered in which a primal-dual active set method, see [20, 21],
 35 is used to solve the finite element approximations. By using Krylov-subspace
 solvers and suitable preconditioners the authors in [22] develop efficient, mesh
 independent, solvers for the (semi-)implicit approximations of \mathcal{P} and $\mathcal{P}_{\mathbf{Q}}$ that
 were derived in [19]. In this work we introduce an alternative preconditioner to
 the ones in [22] resulting in a solver that is not only mesh independent, but also

40 is only mildly dependent of the number of phases N .

We note that in [23] globally convergent nonsmooth Schur–Newton methods are introduced for the solution of discrete multicomponent Cahn–Hilliard systems with logarithmic and obstacle potentials. These methods could also be used to solve the multicomponent Allen–Cahn systems \mathcal{P} and $\mathcal{P}_{\mathbf{Q}}$.

When using iterative techniques to solve the linear system that arises when the primal-dual active set method is used to solve a finite element approximation of $\mathcal{P}_{\mathbf{Q}}$, the majority of the work to be undertaken within each iteration is in the solving of the linear systems $K\mathbf{x} = \mathbf{b}$

$$K = \begin{bmatrix} \mathcal{K} & B^T \\ B & 0 \end{bmatrix},$$

45 where \mathcal{K} is symmetric positive definite. Similar saddle point structures are common place within fluid dynamics, leading to much development of numerical solvers for Navier-Stokes equations, e.g. see [24, 25, 26]. In these papers, it is the choice of preconditioning matrix, P , that leads to improved convergence of the chosen iterative Krylov subspace scheme, e.g. see [27].

50 The preconditioning of the linear systems arising from \mathcal{P} and $\mathcal{P}_{\mathbf{Q}}$ was initially considered in [22], where a preconditioning technique building upon Stokes type systems is proposed. In this work we will use a similar structural approach to that of [22], however, we provide an improved approximation to the Schur complement, $B\mathcal{K}^{-1}B^T$, leading to a solver that is almost independent of the
55 number of phases. Moreover, this improvement does not lead to any significant increase in computational effort per iteration, ultimately leading to a more effective solver. In addition, when considering the two phase problem, with $N = 2$, the minimal polynomial of the resulting preconditioned system is of degree three and hence GMRES will converge within three iterations, see Theorem 3.1.

60 The paper is organised as follows. In Section 2 we reformulate $\mathcal{P}_{\mathbf{Q}}$ with the help of Lagrange multipliers, yielding the associated system $\mathcal{R}_{\mathbf{Q}}$. We then introduce a finite element approximation of an implicit Euler-discretisation of $\mathcal{R}_{\mathbf{Q}}$ and we apply a primal-dual active set algorithm to this discretisation. In

Section 3 a preconditioner for the primal-dual active set algorithm is developed
 65 and the implementation of the numerical solver is presented. In Section 4 we
 present numerical computations that illustrate the effectiveness of our approach,
 in particular they show how the iteration number is independent of the mesh
 size and only mildly dependent on the number of phases N .

s:fea

2. Alternative Formulation and Finite Element Discretisation

70 In this section we follow the authors in [19] in applying a primal-dual active
 set method, [20, 21], to a finite element approximation of $\mathcal{P}_{\mathbf{Q}}$, this method is
 well known in the context of optimisation with partial differential equations as
 constraints. To this end we first reformulate $\mathcal{P}_{\mathbf{Q}}$ with the help of Lagrange
 multipliers, yielding the associated system $\mathcal{R}_{\mathbf{Q}}$, then we apply a Primal Dual
 75 Active Set algorithm to a finite element approximation of $\mathcal{R}_{\mathbf{Q}}$.

2.1. Alternative Formulation of $\mathcal{P}_{\mathbf{Q}}$

In [19] the following alternative formulation of $\mathcal{P}_{\mathbf{Q}}$ is presented:

$\mathcal{R}_{\mathbf{Q}}$: Let $\Omega \subset \mathbb{R}^d$ be a bounded domain which is either convex or fulfills $\partial\Omega \in C^{1,1}$. For given $\mathbf{u}(\cdot, 0) = \mathbf{u}_0 \in \mathcal{G}$, find $\mathbf{u} \in L^2(0, T; \mathbf{H}^2(\Omega)) \cap H^1(0, T; \mathbf{L}^2(\Omega))$,
 80 $\boldsymbol{\mu} \in L^2(0, T; \mathbf{L}^2(\Omega))$, $\boldsymbol{\lambda} \in L^2(0, T; S)$ and $\Lambda \in L^2(0, T; L^2(\Omega))$ such that

$$\begin{aligned} \varepsilon \frac{\partial \mathbf{u}}{\partial t} - \varepsilon \Delta \mathbf{u} - \frac{1}{\varepsilon} \mathbf{A} \mathbf{u} - \frac{1}{\varepsilon} \boldsymbol{\mu} - \frac{1}{\varepsilon} \Lambda \mathbf{1} - \frac{1}{\varepsilon} \boldsymbol{\lambda} &= \mathbf{0} \text{ a.e. in } \Omega \times (0, T), \\ \mathbf{u} \cdot \mathbf{1} &= 1 \text{ a.e. in } \Omega \times (0, T), \\ (\mathbf{u}, 1) = \mathbf{Q}, (\boldsymbol{\mu}, \mathbf{u}) &= 0, \text{ for almost all } t \in (0, T), \\ \mathbf{u} \geq \mathbf{0}, \boldsymbol{\mu} &\geq \mathbf{0}, \text{ a.e. in } \Omega \times (0, T). \end{aligned}$$

Here the Lagrange multipliers $\boldsymbol{\mu}$, Λ and $\boldsymbol{\lambda}$ are such that

- (i) $\boldsymbol{\mu}(\mathbf{x}, t) : \Omega \times (0, T) \rightarrow \mathbb{R}^N$, is used to impose the constraint $\mathbf{u} \geq \mathbf{0}$,
- (ii) $\boldsymbol{\lambda}(t) : \mathbb{R}^N \times (0, T) \rightarrow S$, is used to impose the mass constraint $\int_{\Omega} \mathbf{u} \, d\mathbf{x} = \mathbf{Q}$,
- (iii) $\Lambda(\mathbf{x}, t) : \Omega \times (0, T) \rightarrow \mathbb{R}$, is used to impose the saturation constraint
 85 $\mathbf{u} \cdot \mathbf{1} = 1$,

and $S := \{\mathbf{v} \in \mathbb{R}^N : \mathbf{v} \cdot \mathbf{1} = 0\}$.

$\mathcal{R}_{\mathbf{Q}}$ is complemented with the boundary condition $\frac{\partial \mathbf{u}}{\partial \nu} = 0$, where ν is the outer unit normal to $\partial\Omega$.

Remark 2.1. *The scaling $\frac{1}{\varepsilon}\boldsymbol{\mu}$ in $\mathcal{R}_{\mathbf{Q}}$ is introduced in order that $\boldsymbol{\mu}$ is of order one, if we were to replace $\frac{1}{\varepsilon}\boldsymbol{\mu}$ by $\boldsymbol{\mu}$ we would observe a severe ε -dependence of $\boldsymbol{\mu}$ which in practice often results in oscillations in the discretised primal-dual active set method.*

2.2. Finite Element Discretisation

For simplicity we assume that Ω is a polyhedral domain. Let \mathcal{T}_h be a regular triangulation of Ω into disjoint open simplices, i.e. in particular $\bar{\Omega} = \cup_{T \in \mathcal{T}_h} \bar{T}$. Furthermore, we define $h := \max_{T \in \mathcal{T}_h} \{\text{diam } T\}$ the maximal element size of \mathcal{T}_h and we set \mathcal{J} to be the set of nodes of \mathcal{T}_h and $\{\mathbf{p}_j\}_{j \in \mathcal{J}}$ to be the coordinates of these nodes. Associated with \mathcal{T}_h is the piecewise linear finite element space

$$S_h := \left\{ \varphi \in C^0(\bar{\Omega}) \mid \varphi|_T \in P_1(T) \ \forall T \in \mathcal{T}_h \right\} \subset H^1(\Omega),$$

where we denote by $P_1(T)$ the set of all affine linear functions on T . Furthermore we denote the standard nodal basis functions of S_h by $\{\chi_j\}_{j \in \mathcal{J}}$ and we set $\mathbf{S}_h = (S_h)^N$.

The time domain $(0, T)$ is divided into N_T uniform intervals (t_{n-1}, t_n) , with $\tau := t_n - t_{n-1}$, $n = 1, 2, \dots, N_T$. For simplicity of presentation we denote by $\mathbf{u}_h \in \mathbf{S}_h$ the discrete solution at time t_n , while the solution at the previous time step will be denoted by $\mathbf{u}_h^{n-1} \in \mathbf{S}_h$, and similarly for $\boldsymbol{\mu}_h$, $\boldsymbol{\lambda}_h$ and Λ_h .

We consider the following fully discrete approximation of $\mathcal{R}_{\mathbf{Q}}$:

$\mathcal{R}_{\mathbf{Q}}^{h,\tau}$ Given $\mathbf{u}_h^{n-1} \in \mathbf{S}_h$, find $\mathbf{u}_h \in \mathbf{S}_h$, $\boldsymbol{\mu}_h \in \mathbf{S}_h$, $\boldsymbol{\lambda}_h \in \mathbb{R}^N$ and $\Lambda_h \in S_h$ such

that

$$\begin{aligned} & \frac{\varepsilon^2}{\tau}(\mathbf{u}_h, \boldsymbol{\chi})_h + \varepsilon^2(\nabla \mathbf{u}_h, \nabla \boldsymbol{\chi}) - (\boldsymbol{\mu}_h, \boldsymbol{\chi})_h - (\boldsymbol{\lambda}_h, \boldsymbol{\chi}) - (\Lambda_h \mathbf{1}, \boldsymbol{\chi})_h \\ &= \frac{\varepsilon^2}{\tau}(\mathbf{u}_h^{n-1}, \boldsymbol{\chi})_h + (\mathbf{A} \mathbf{u}_h^{n-1}, \boldsymbol{\chi})_h \quad \forall \boldsymbol{\chi} \in \mathbf{S}_h, \end{aligned} \tag{1} \quad \text{eq2a}$$

$$\sum_{i=1}^N (u_i)_j = 1 \quad \forall j \in \mathcal{J}, \tag{2} \quad \text{eq2b1}$$

$$\sum_{j \in \mathcal{J}} M_j((u_i)_j - (u_N)_j) = \sum_{j \in \mathcal{J}} M_j(m_i - m_N) \quad \text{for } i \in \{1, \dots, N-1\}, \tag{3} \quad \text{eq2b}$$

$$\lambda_N = - \sum_{i=1}^{N-1} \lambda_i, \tag{4} \quad \text{eq2lam}$$

$$\boldsymbol{\mu}_j \geq \mathbf{0}, \quad \mathbf{u}_j \geq \mathbf{0} \quad \forall j \in \mathcal{J}, \quad (\mathbf{u}_h, \boldsymbol{\mu}_h)_h = 0. \tag{5} \quad \text{eq:cons2a}$$

Here $(u_i)_j$ denotes the i -th component u_i of \mathbf{u} at the j -th node, $(f, g)_h = \int_{\Omega} I_h(fg)$ denotes the lumped mass semi-inner product where $I_h : C^0(\overline{\Omega}) \rightarrow S_h$ is the standard interpolation operator such that $(I_h f)(\mathbf{p}_j) = f(\mathbf{p}_j)$ for all nodes $j \in \mathcal{J}$ and $M_j := (\chi_j, \chi_j)_h$, $j \in \mathcal{J}$.

Remark 2.2. Due to the $\mathbf{A} \mathbf{u}$ term in $\mathcal{P}_{\mathbf{Q}}$, the problem is non-convex, in the above discretisation we have chosen to treat this term fully explicitly. Alternative choices would be to treat this term fully implicitly, or in a semi-implicit manner, neither of which would affect the performance of our proposed solver.

2.3. The Primal Dual Active Set Method

We use the nonlinear primal dual active set (PDAS) algorithm derived in [19] to solve $\mathcal{R}_{\mathbf{Q}}^{h, \tau}$. The algorithm is obtained by reformulating the complementarity conditions (5) using active sets based on the primal variable \mathbf{u} and the dual variable $\boldsymbol{\mu}$. Here we use the notation $(u_i^k)_j$ and $(u_i^{n-1})_j$ where k denotes the k -th iteration in the PDAS algorithm and $n-1$ is the $(n-1)$ -st time step. This is of course a misuse of notation for $k = n-1$. In addition for $c > 0$, we set

$$\mathcal{A}_i^{k+1} := \{j \in \mathcal{J} : c \cdot (u_i^k)_j - (\mu_i^k)_j < 0\},$$

and we define the lumped mass diagonal matrix $M := (m_{ij})_{i,j \in \mathcal{J}}$ with $m_{ij} = (\chi_i, \chi_j)_h$ and the stiffness matrix $L := (l_{ij})_{i,j \in \mathcal{J}}$ with $l_{ij} = (\nabla \chi_j, \nabla \chi_i)$. We define the mass lumped vector $\mathbf{m} := (M_j)_{j \in \mathcal{J}}$, and the entries of the matrix \mathbf{A} by $a_{ij}, i, j = \{1, \dots, N\}$.

Primal-Dual Active Set Algorithm (PDAS):

0. Set $k = 0$ and initialise $\mathcal{A}_i^0 \subset \mathcal{J}$ for all $i \in \{1, \dots, N\}$.
1. Define $\mathcal{I}_i^k = \mathcal{J} \setminus \mathcal{A}_i^k$ for all $i \in \{1, \dots, N\}$.
 Set $(u_i^k)_j = 0$ for $j \in \mathcal{A}_i^k$, $(u_i^k)_j = 1$ for $j \in \mathcal{I}_i^k \setminus \mathcal{D}_i^k$ and $(\mu_i^k)_j = 0$ for $j \in \mathcal{I}_i^k$ for all $i \in \{1, \dots, N\}$.
2. Set $\mathcal{D}_i^k := \mathcal{I}_i^k \cap (\bigcup_{\substack{j=1 \\ j \neq i}}^N \mathcal{I}_j^k)$, $\mathcal{D}^k := \bigcup_{i=1}^N \mathcal{D}_i^k$. Solve the discretised PDE (1) on the interface \mathcal{D}^k with the constraints (2)-(4) to obtain $(u_i^k)_j$ for all (i, j) such that $j \in \mathcal{D}_i^k, i \in \{1, \dots, N\}$, Λ_j^k for all $j \in \mathcal{D}^k$, and λ_i^k for all $i \in \{1, \dots, N\}$. More precisely we solve

$$\frac{\varepsilon^2}{\tau}(u_i^k)_j + \frac{\varepsilon^2}{M_j} \sum_{r \in \mathcal{J}} l_{rj}(u_i^k)_r - \lambda_i^k - \Lambda_j^k = \frac{\varepsilon^2}{\tau}(u_i^{n-1})_j + \sum_{m=1}^N a_{im}(u_m^{n-1})_j$$

for $j \in \mathcal{D}_i^k$ and $i \in \{1, \dots, N\}$,

(6) pdas1

$$\sum_{i=1}^N (u_i^k)_j = 1 \text{ for } j \in \mathcal{D}^k,$$
(7) pdas3

$$\sum_{j \in \mathcal{J}} M_j((u_i^k)_j - (u_N^k)_j) = \sum_{j \in \mathcal{J}} M_j(m_i - m_N) \text{ for } i \in \{1, \dots, N-1\},$$
(8) pdas2

where $\lambda_N^k = -\sum_{i=1}^{N-1} \lambda_i^k$ is used in (6).

3. Define Λ_j^k for all $j \in \mathcal{I}_i^k \setminus \mathcal{D}^k$ as

$$\Lambda_j^k = \frac{\varepsilon^2}{\tau}(u_i^k)_j + \frac{\varepsilon^2}{M_j} \sum_{r \in \mathcal{J}} l_{rj}(u_i^k)_r - \lambda_i^k - \frac{\varepsilon^2}{\tau}(u_i^{n-1})_j + \sum_{m=1}^N a_{im}(u_m^{n-1})_j.$$

4. Determine $(\mu_i^k)_j$ for $j \in \mathcal{A}_i^k$ using (1) for all $i = 1, \dots, N$ as

$$(\mu_i^k)_j = \frac{\varepsilon^2}{\tau}(u_i^k)_j + \frac{\varepsilon^2}{M_j} \sum_{r \in \mathcal{J}} l_{rj}(u_i^k)_r - \lambda_i^k - \Lambda_j^k - \frac{\varepsilon^2}{\tau}(u_i^{n-1})_j + \sum_{m=1}^N a_{im}(u_m^{n-1})_j.$$

130 5. Set $\mathcal{A}_i^{k+1} := \{j \in \mathcal{J} : c(u_i^k)_j - (\mu_i^k)_j < 0\}$ for $i \in \{1, \dots, N\}$.

6. If $\mathcal{A}_i^{k+1} = \mathcal{A}_i^k$ for all $i \in \{1, \dots, N\}$ stop, otherwise set $k = k + 1$ and goto 1.

Remark 2.3. In [19] the authors show local convergence of the Primal Dual Active Set method, however as they mention in Remark 4.7, the convergence
135 radius is unknown. In practice the oscillatory behaviour of the method can occur if c is not chosen appropriately, in Section 4D of [28] an example of the scalar case, $N = 2$, in one space-dimension, with $\Omega = (-1, 1)$, is presented in which oscillatory behaviour of the method is observed if c is chosen to be less than $\frac{1}{h^2}$. In what follows we take $c = \frac{2}{h^2}$, which led to good convergence in all
140 the computations presented in Section 4.

3. Preconditioning

s:precon

3.1. Schur Complement

The main computational cost in the above algorithm is the solving of the system of equations (6), (8) and (7). To do this we firstly introduce some matrix notation. At the k -th iteration step we define \mathcal{K}^k , to be N diagonal blocks with the i -th block, \mathcal{K}_i^k , being associated with the active set, \mathcal{D}_i^k , of the i -th phase equation of (6). More precisely,

$$\mathcal{K}_i^k := \frac{\varepsilon^2}{\tau}(m_{rj})_{r \in \mathcal{J}, j \in \mathcal{D}^k} + \varepsilon^2(l_{rj})_{r \in \mathcal{J}, j \in \mathcal{D}^k}.$$

We further define,

$$\mathcal{B}_1^k := \begin{bmatrix} -(\mathbf{m}_1^k)^T & 0 & 0 & \dots & (\mathbf{m}_N^k)^T \\ 0 & -(\mathbf{m}_2^k)^T & 0 & \dots & (\mathbf{m}_N^k)^T \\ & & \dots & & \\ 0 & 0 & \dots & -(\mathbf{m}_{N-1}^k)^T & (\mathbf{m}_N^k)^T \end{bmatrix} \in \mathbb{R}^{N-1 \times \omega^k},$$

where $\omega^k = \sum_{i=1}^N |D_i^k|$ and

$$\mathcal{B}_2^k := [-M_1^k, -M_2^k, \dots, -M_N^k] \in \mathbb{R}^{|\mathcal{J}| \times \omega^k}.$$

At the k -th iteration, we may write this linear system in the form; find $\mathbf{x}^k := [\mathbf{u}^k, \boldsymbol{\lambda}^k, \Lambda^k]$ such that $K^k \mathbf{x}^k = \mathbf{b}^k$, where the coefficient matrix is of the

145 form

$$K^k := \begin{bmatrix} \mathcal{K}^k & (\mathcal{B}_1^k)^T & (\mathcal{B}_2^k)^T \\ \mathcal{B}_1^k & 0 & 0 \\ \mathcal{B}_2^k & 0 & 0 \end{bmatrix}. \quad (9)$$

For convenience, from here on we will drop the superscript k .

To develop a preconditioner for K , we write it in the factored form

$$K = \begin{bmatrix} I & 0 & 0 \\ \mathcal{B}_1 \mathcal{K}^{-1} & I & 0 \\ \mathcal{B}_2 \mathcal{K}^{-1} & 0 & I \end{bmatrix} \begin{bmatrix} \mathcal{K} & \mathcal{B}_1^T & \mathcal{B}_2^T \\ 0 & \mathcal{S}_{11} & \mathcal{S}_{12} \\ 0 & \mathcal{S}_{21} & \mathcal{S}_{22} \end{bmatrix},$$

where $\mathcal{S}_{ij} := -\mathcal{B}_i \mathcal{K}^{-1} \mathcal{B}_j^T$ for $i, j = 1, 2$. Rearranging gives,

$$\begin{bmatrix} \mathcal{K} & \mathcal{B}_1^T & \mathcal{B}_2^T \\ \mathcal{B}_1 & 0 & 0 \\ \mathcal{B}_2 & 0 & 0 \end{bmatrix} \begin{bmatrix} \mathcal{K} & \mathcal{B}_1^T & \mathcal{B}_2^T \\ 0 & \mathcal{S}_{11} & \mathcal{S}_{12} \\ 0 & \mathcal{S}_{21} & \mathcal{S}_{22} \end{bmatrix}^{-1} = \begin{bmatrix} I & 0 & 0 \\ \mathcal{B}_1 \mathcal{K}^{-1} & I & 0 \\ \mathcal{B}_2 \mathcal{K}^{-1} & 0 & I \end{bmatrix}.$$

Hence, if we choose the preconditioner

$$\mathcal{P}_{\text{exact}} := \begin{bmatrix} \mathcal{K} & \mathcal{B}_1^T & \mathcal{B}_2^T \\ 0 & \mathcal{S}_{11} & \mathcal{S}_{12} \\ 0 & \mathcal{S}_{21} & \mathcal{S}_{22} \end{bmatrix},$$

the eigenvalues of the preconditioned system have value one, and it can be shown

150 that only two GMRES iterations would be needed in this case, see [24].

Since each block of \mathcal{K} consists of the standard finite element matrix for a reaction-diffusion type equation, there exists numerous practical preconditioners and solvers for this block. In particular standard algebraic, or geometric,

multigrid can effectively be applied, see [29, 30]. Hence, we are left to find a fully practical approximation to the action of the block matrix

$$S_{\text{exact}} := \begin{bmatrix} \mathcal{S}_{11} & \mathcal{S}_{12} \\ \mathcal{S}_{21} & \mathcal{S}_{22} \end{bmatrix}.$$

3.2. Approximate Schur Preconditioners

In [22] the authors consider a block upper triangular preconditioner of the form:

$$P_1 := \begin{bmatrix} \mathcal{K} & \mathcal{B}_1^T & \mathcal{B}_2^T \\ 0 & \tilde{\mathcal{S}}_{11} & 0 \\ 0 & 0 & \tilde{\mathcal{S}}_{22} \end{bmatrix}, \quad (10) \quad \boxed{\text{p1}}$$

where the diagonal blocks $\tilde{\mathcal{S}}_{ii}$, $i = 1, 2$ are given by

$$\tilde{\mathcal{S}}_{11} := \frac{1}{N} \mathcal{M} \mathcal{K}^{-1} \mathcal{M} \text{ and } \tilde{\mathcal{S}}_{22} := (\mathbf{1} \cdot \mathbf{1}^T + I),$$

where I is the identity matrix. This choice was shown to lead to the preconditioned system

$$K P_1^{-1} = \begin{bmatrix} I & 0 & 0 \\ 0 & I + E_{11} & E_{12} \\ 0 & E_{21} & I + E_{22} \end{bmatrix},$$

where E_{ii} , $i = 1, 2$, are such that all eigenvalues are close to zero. Note that with this choice of preconditioner, $\tilde{\mathcal{S}}_{ij} = 0$, $i \neq j$, and hence in [22] the effect of the off diagonal blocks is not considered.

155 In this work we propose an alternative approximation by building on the ideas presented in [31]. We firstly define, $B := [\mathcal{B}_1, \mathcal{B}_2]^T$, leading to $S_{\text{exact}} = B \mathcal{K}^{-1} B^T$. Following [31] we approximate this with

$$\begin{aligned} S_{\text{exact}} &\approx (B B^T) (B \mathcal{K} B^T)^{-1} (B B^T), \\ &= \begin{bmatrix} \mathcal{B}_1 \mathcal{B}_1^T & \mathcal{B}_1 \mathcal{B}_2^T \\ \mathcal{B}_2 \mathcal{B}_1^T & \mathcal{B}_2 \mathcal{B}_2^T \end{bmatrix} (B \mathcal{K} B^T)^{-1} \begin{bmatrix} \mathcal{B}_1 \mathcal{B}_1^T & \mathcal{B}_1 \mathcal{B}_2^T \\ \mathcal{B}_2 \mathcal{B}_1^T & \mathcal{B}_2 \mathcal{B}_2^T \end{bmatrix} \\ &:= \begin{bmatrix} D_{11} & D_{12} \\ D_{21} & D_{22} \end{bmatrix} (B \mathcal{K} B^T)^{-1} \begin{bmatrix} D_{11} & D_{12} \\ D_{21} & D_{22} \end{bmatrix} := D (B \mathcal{K} B^T)^{-1} D. \quad (11) \end{aligned}$$

Note that,

$$D_{11} = \begin{bmatrix} \alpha_1 + \alpha_N & \alpha_N & \alpha_N & \dots & \alpha_N \\ \alpha_N & \alpha_2 + \alpha_N & \alpha_N & \dots & \alpha_N \\ \dots & \dots & \dots & \dots & \dots \\ \alpha_N & \alpha_N & \dots & \dots & \alpha_{N-1} + \alpha_N \end{bmatrix} \in \mathbb{R}^{N-1 \times N-1},$$

where $\alpha_i = \mathbf{m}_i^T \mathbf{m}_i, i = 1, 2, \dots, N$ and

$$D_{22} = \sum_{i=1}^N M_i M_i^T \in \mathbb{R}^{|\mathcal{J}| \times |\mathcal{J}|}.$$

Remark 3.1. *How well this preconditioner performs is closely related to how well B commutes with \mathcal{K} . We note that the matrix D_{22} is diagonal. Moreover, it is a relatively large proportion of the matrix B , and will always be close to a constant diagonal matrix in the regions $\mathcal{D}_i^{n,k}$. This will even be the case when an adaptive mesh refinement strategy is used to accurately capture the interfacial region, since in this active region the elements are of similar size and shape. Hence, the commutator of $[D_{22}, C]$, with any square matrix C is close to zero. This is a major factor in the quality of the approximation used in (11).*

We consider two preconditioners developed from the above methodology. Namely, the block diagonal choice

$$P_2 := \begin{bmatrix} \mathcal{K} & \mathcal{B}_1^T & \mathcal{B}_2^T \\ 0 & D_{11}(\mathcal{B}_1 \mathcal{K} \mathcal{B}_1^T)^{-1} D_{11} & 0 \\ 0 & 0 & D_{22}(\mathcal{B}_2 \mathcal{K} \mathcal{B}_2^T)^{-1} D_{22} \end{bmatrix}, \quad (12) \quad \boxed{\text{p2}}$$

and the full approximation

$$P_3 := \begin{bmatrix} \mathcal{K} & B^T \\ 0 & D(B \mathcal{K} B^T)^{-1} D \end{bmatrix}. \quad (13) \quad \boxed{\text{p3}}$$

3.3. Practical Preconditioning

The implementation of any of the preconditioners $P_i, i = 1, 2, 3$, requires a practical and scalable method to calculate the action of their inverses. All three

preconditioners have inverses that may be written in the form,

$$P_i^{-1} := \begin{bmatrix} \mathcal{K}^{-1} & 0 \\ 0 & I \end{bmatrix} \begin{bmatrix} I & B^T \\ 0 & -I \end{bmatrix} \begin{bmatrix} I & 0 \\ 0 & \mathcal{S}_i^{-1} \end{bmatrix}, \quad \text{for } i = 1, 2, 3$$

where

$$\mathcal{S}_1 := \begin{bmatrix} \tilde{\mathcal{S}}_{11} & 0 \\ 0 & \tilde{\mathcal{S}}_{22} \end{bmatrix}, \quad \mathcal{S}_2 := \begin{bmatrix} D_{11}(\mathcal{B}_1 \mathcal{K} \mathcal{B}_1^T)^{-1} D_{11} & 0 \\ 0 & D_{22}(\mathcal{B}_2 \mathcal{K} \mathcal{B}_2^T)^{-1} D_{22} \end{bmatrix}$$

and

$$\mathcal{S}_3 := D(B \mathcal{K} B^T)^{-1} D.$$

The main work in calculating the action of these inverses is in calculating the action of the inverses of \mathcal{K} and $\mathcal{S}_i, i = 1, 2, 3$. As mentioned earlier, for the matrix \mathcal{K} numerous efficient iterative solvers exist. In the following numerical results section we chose to apply three Algebraic Multigrid (AMG) V-cycles with simple Gauss-Seidel smoothing, see [30].

For \mathcal{S}_1 and \mathcal{S}_2 we are only required to invert a small dense matrix $\tilde{\mathcal{S}}_{11}$ and in finding the action of the inverse $\tilde{\mathcal{S}}_{22}$ we only require the inversion of the diagonal lumped mass matrix. Finally, for \mathcal{S}_3 we write,

$$D^{-1} = \begin{bmatrix} I & 0 \\ -D_{22}^{-1} D_{21} & I \end{bmatrix} \begin{bmatrix} (D_{11} - D_{12} D_{22}^{-1} D_{21})^{-1} & 0 \\ 0 & D_{22}^{-1} \end{bmatrix} \begin{bmatrix} I & -D_{12} D_{22}^{-1} \\ 0 & I \end{bmatrix}.$$

We note from earlier remarks that the construction of the matrix $D_{11} - D_{12} D_{22}^{-1} D_{21} \in \mathbb{R}^{N-1 \times N-1}$ and its inverse is inexpensive.

3.4. The Two Phase Problem

175

theorem

Theorem 3.1. *When considering a two phase problem, the right preconditioners P_2 and P_3 are identical. Moreover, the resulting preconditioned system, $K P_i^{-1}$, $i = 2, 3$, is a lower triangular matrix with the diagonal consisting of 1's and a solitary*

$$a = \frac{\mathbf{m}_1^T \mathcal{K}_1^{-1} \mathbf{m}_1}{(\mathbf{m}_1^T \mathbf{m}_1) (\mathbf{m}_1^T \mathcal{K}_1 \mathbf{m}_1)^{-1} (\mathbf{m}_1^T \mathbf{m}_1)}.$$

Furthermore, the minimal polynomial of the resulting system is of degree three and hence GMRES will converge within three iterations.

Proof: In the two phase case the system to be solved is of the form

$$K := \begin{bmatrix} \mathcal{K} & (\mathcal{B}_1)^T & (\mathcal{B}_2)^T \\ \mathcal{B}_1 & 0 & 0 \\ \mathcal{B}_2 & 0 & 0 \end{bmatrix},$$

where

$$\mathcal{B}_1 = \begin{bmatrix} -\mathbf{m}_1^T & \mathbf{m}_1^T \end{bmatrix}, \quad \mathcal{B}_2 = \begin{bmatrix} -M_1 & -M_1 \end{bmatrix} \quad \text{and} \quad \mathcal{K} = \begin{bmatrix} \mathcal{K}_1 & 0 \\ 0 & \mathcal{K}_1 \end{bmatrix}.$$

This leads to the exact Schur complement,

$$\mathcal{S}_{exact} = \begin{bmatrix} -2\mathbf{m}_1^T \mathcal{K}_1^{-1} \mathbf{m}_1 & 0 \\ 0 & -2M_1 \mathcal{K}_1^{-1} M_1 \end{bmatrix}.$$

Moreover, since $\mathcal{B}_1 \mathcal{B}_2^T = 0$,

$$\mathcal{S}_2 = \mathcal{S}_3 = \begin{bmatrix} -2(\mathbf{m}_1^T \mathbf{m}_1) (\mathbf{m}_1^T \mathcal{K}_1 \mathbf{m}_1)^{-1} (\mathbf{m}_1^T \mathbf{m}_1) & 0 \\ 0 & -2M_1 \mathcal{K}_1^{-1} M_1 \end{bmatrix}.$$

Hence,

$$\mathcal{S}_{exact} \mathcal{S}_i^{-1} = \begin{bmatrix} a & 0 \\ 0 & I \end{bmatrix}, \quad i = 2, 3,$$

where a is a scalar. This leads to the full preconditioned system

$$K P_2^{-1} = \begin{bmatrix} I & 0 & 0 & 0 \\ 0 & I & 0 & 0 \\ -\mathbf{m}_1^T \mathcal{K}_1^{-1} & \mathbf{m}_1^T \mathcal{K}_1^{-1} & a & 0 \\ -M_1^T \mathcal{K}_1^{-1} & -M_1^T \mathcal{K}_1^{-1} & 0 & I \end{bmatrix}.$$

Clearly, this system has only two distinct eigenvalues, $\sigma(K P_2^{-1}) = \{1, a\}$ and the minimum polynomial for this preconditioned system is of order three. Hence,

when using GMRES we would expect to obtain the exact solution in no more than three iterations, see [32].

4. Numerical Results

In this section we present numerical results that show the efficiency of our proposed preconditioner P_3 , (13). We begin by using exact solves for each matrix in the preconditioning system, then in later results we apply three Algebraic Multigrid (AMG) V-cycles with simple Gauss-Seidel smoothing, see [30], for calculating the action of the inverse of \mathcal{K} . We denote the approximate preconditioners, in which we use the inexact AMG solver, by $P_{i,AMG}$, $i = 1, 2, 3$.

We note that the fully explicit discretisation of \mathbf{A} in $\mathcal{R}_{\mathbf{Q}}^{h,\tau}$ leads to an unconditionally well posed discrete problem, allowing the use of large time steps when slow dynamics are encountered, see [16]. Regarding time stepping, throughout we will use a simple adaptive time stepping strategy whereby:

1. If the number of PDAS steps required to obtain \mathbf{u}^{n+1} are fewer than 5, we set $\tau_{n+1} = 1.1\tau_n$.
2. If the number of PDAS steps required to obtain \mathbf{u}^{n+1} is between 5 and 10, τ_n remains unchanged.
3. If the number of PDAS steps required to obtain \mathbf{u}^{n+1} exceeds 10, we recalculate \mathbf{u}^{n+1} with a time step reduced by a half, $\tau_n = 0.5\tau_n$.

At time step n with initial time step τ_n and previous solution \mathbf{u}^n using the PDAS iteration scheme calculate \mathbf{u}^{n+1} . This solution is taken when the active set size does not change between iterations. We found that this led to a practical stable method.

In all computations we set $c = \frac{2}{h^2}$. In two space dimensions we set $\Omega = [0, 1]^2$ and in three space dimensions we set $\Omega = [-0.5, 0.5]^3$.

Remark 4.1. 1. *Since the interfacial thickness is proportional to ε , in order to resolve the interfacial layer, we need to choose the mesh size h such that $h \ll \varepsilon$, see [6] for details. In all computations, with the exception of those in Section 4.1.1, the values of h that we used were sufficient to resolve*

the interfacial layer. For the results in Section 4.1.1, in which successive uniform refinements of an initial coarse mesh were used to produce finer meshes, it was not practical to use a value of h that, in the case of the initial coarse mesh, successfully resolved the interfacial region for all the specified values of ε . However when performing the computations, the fact that the interfacial regions were not fully resolved on the coarse mesh, did not appear to impact on the performance of the solvers or on the interface dynamics.

2. During initial calculations, it was seen that the proposed PDAS scheme was only reliable when a high tolerance was enforced on linear solve. Hence, throughout the following results we will apply a tolerance on the relative GMRES error of $1e-10$. Given this constraint on the PDAS scheme, it is critical that a robust and efficient solver is used.

4.1. Two Space Dimensions

4.1.1. Grain Coarsening

The first problem we consider is that of grain coarsening in which we start with an initially well mixed mixture of N phases. The mixture rapidly separates into bulk regions of each phase, with typically each phase having multiple bulk regions. Once this fast dynamical process has taken place, the bulk regions then slowly diffuse, see Figure 1 where the motion of eight phases from $T = 1$ to $T = 100$ is presented.

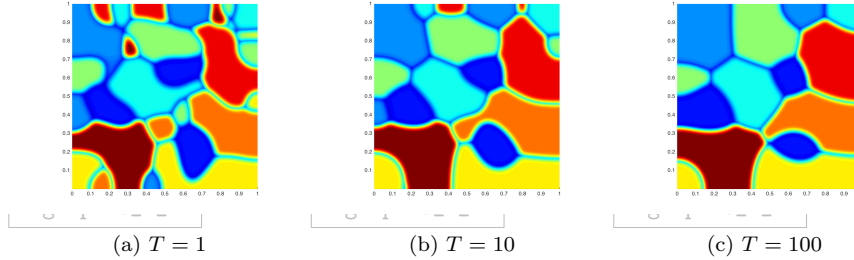


Figure 1: Evolution of eight initially well mixed phases.

fig: evolution

Two Phases									
	Mesh 1 ($ \mathcal{J} = 3765$)			Mesh 2 ($ \mathcal{J} = 14889$)			Mesh 3 ($ \mathcal{J} = 59217$)		
ε	P_1	P_2	P_3	P_1	P_2	P_3	P_1	P_2	P_3
0.04	35/ 24	3	3	29/ 21	3	3	25/ 20	3	3
0.02	36/ 24	3	3	31/ 25	3	3	27/ 24	3	3
0.01	36/ 22	3	3	31/ 26	3	3	28/ 26	3	3

Four Phases									
ε	P_1	P_2	P_3	P_1	P_2	P_3	P_1	P_2	P_3
0.04	70/ 49	17/ 12	10/ 8	64/ 42	18/ 12	13/ 10	62/ 40	17/ 13	11/ 10
0.02	64/ 47	15/ 13	9/ 8	64/ 50	16/ 13	10/ 9	62/ 45	18/ 12	12/ 11
0.01	60/ 41	14/ 13	8/ 7	58/ 49	15/ 14	10/ 8	61/ 47	18/ 13	11/ 9

Six Phases									
ε	P_1	P_2	P_3	P_1	P_2	P_3	P_1	P_2	P_3
0.04	92/ 57	22/ 15	12/ 9	84/ 63	25/ 16	15/ 10	89/ 49	24/ 18	11/ 10
0.02	88/ 65	21/ 17	9/ 8	85/ 65	21/ 17	13/ 11	95/ 66	23/ 17	12/ 10
0.01	75/ 55	18/ 17	9/ 7	75/ 65	21/ 18	12/ 10	91/ 61	22/ 17	12/ 10

Table 1: Maximum GMRES iteration counts for the exact preconditioners P_1 , P_2 and P_3 when starting with a well mixed initial condition.

tab: spin 2D

We compare the performance of the three exact preconditioners P_1 , (10), P_2 , (12), and P_3 , (13), with respect to: the number of phases, the interface width parameter ε , and the mesh size. In each case we use exact solves for each matrix in the preconditioning system. The initial mesh, Mesh 1, has mesh size $h \approx 1/32$ and all other meshes are uniform refinements of this mesh, the number of nodes of each mesh is given by $|\mathcal{J}|$. In Table 1 we display the maximum number of GMRES iteration counts together with the average number, in the form a/\mathbf{b} , where a is the maximum number and \mathbf{b} is the average number. We consider three meshes, three values of ε , and three values of N . From this table, for each of the three meshes and each of the three values of ε , we see the dependence of P_1 on the number of phases, N . A similar dependence can be seen for the choice P_2 , albeit a milder one. It is P_3 that outperforms the other two choices in this regard, as it shows almost no dependence on phase number for each of the three meshes and each of the three values of ε . In addition, for the two phase problem, $N = 2$, we observe the three iteration convergence, stated in Theorem 3.1.

In Figure 2 we further investigate how the number of phases, N , affects the performance of exact preconditioners P_1 and P_3 . We ignore P_2 since P_3 is computationally similar whilst having superior convergence rates. We display the number of GMRES iterations throughout a simulation together with the percentage of the total number of DOFs that the inactive sets make up. In addition we show the effect of the active time stepping by displaying the time step size throughout the simulation. We set $\varepsilon = 0.01$ and use Mesh 4, which has $|\mathcal{J}| = 236868$. Similar to Table 1, we see a strong dependence for P_1 but a very weak dependence for P_3 . The results in Figure 3 are displayed in the same format as those in Figure 2, but here we investigate the effect that the mesh size has on the performance of preconditioners P_1 and P_3 . In particular we set $\varepsilon = 0.02$ and $N = 4$ and we show results for Mesh 3, for which $|\mathcal{J}| = 59217$, and Mesh 4. We conclude with Figure 4 in which we set $N = 4$ and use Mesh 4, with $\varepsilon = 0.02$ and $\varepsilon = 0.01$ to see the effect that ε has on the performance of preconditioners P_1 and P_3 . In both Figures 3 and 4 we again see a strong

Two Phases - 3D			
ε	Mesh 1 ($ \mathcal{J} = 17576$)	Mesh 2 ($ \mathcal{J} = 29791$)	Mesh 3 ($ \mathcal{J} = 68921$)
0.04	3	3	3
0.02	3	3	3
Four Phases - 3D			
0.04	13/ 7	11/ 7	10/ 7
0.02	11/ 6	9/ 6	9/ 6
Six Phases - 3D			
0.04	14/ 9	10/ 7	8/ 6
0.02	10/ 5.5	9/ 7	9/ 6.5

Table 2: Maximum GMRES iteration counts when starting with a well mixed initial condition, using the exact preconditioner, P_3 .

tab: spin 3D

dependence for P_1 but a very weak dependence for P_3 .

4.1.2. Quadruple Junction to Triple Junction

265 We now turn to an initial condition of fully formed bulk regions. We set $\varepsilon = 0.005$ and $N = 5$. For the initial data we consider a square, consisting of four phases of bulk square regions, that is surrounded by a fifth phase. This unstable initial geometry rapidly evolves so that the quadruple junction is replaced by two triple junctions with 120° angles, see Figure 5.

270 In Figure 6 we present the iteration counts and inactive set size when using the inexact preconditioner $P_{3,AMG}$. Given the maximum number of iteration counts for a given time step is only 11, we conclude that the use of the inexact *AMG* solver on the \mathcal{K} block has little effect on proposed solver.

4.2. Three Space Dimensions

275 4.2.1. Grain Coarsening

In Table 2 we present the GMRES iteration counts when using the exact preconditioner P_3 . As in the two dimensional case, we see that there is little de-

$\varepsilon = 0.04$			
	Mesh 1 ($ \mathcal{J} = 9261$)	Mesh 2 ($ \mathcal{J} = 29791$)	Mesh 3 ($ \mathcal{J} = 68921$)
$N = 2$	72s	342s	1133s
$N = 4$	135s	824s	2961s
$N = 6$	284s	1324s	8356s

Table 3: CPU timings using the inexact preconditioner $P_{3,AMG}$ in three space dimensions. Initial condition is well mixed and $T = 2$.

tab: AMG 3D

pendence on any of the parameters, mesh size, ε , or number of phases, and again we observe the three iteration convergence of the two phase problem. Turning
280 to the fully practical inexact preconditioner, $P_{3,AMG}$, in Table 3 we present CPU timings for this problem. It is not clear how to measure how these timings scale, since as the mesh is refined and more phases are added, the inactive set size changes considerably. However, we feel that these non-optimized CPU timings are an excellent indicator of the scalability of the proposed approach.

285 Finally, for the well mixed problem we consider an initial problem of a well mixed sphere of 8 phases surrounded by a final pure 9-th phase, we take $\varepsilon = 0.04$. The mesh used has over a half a million nodes, this leads to a system size of more than five million degrees of freedom. The evolution of these phases can be seen in Figure 7, while Figure 8 displays the iteration counts and inactive set
290 size.

4.2.2. Quadruple Junction to Triple Junction

Finally, we consider a three dimensional problem analogous to the two dimensional quadruple junction problem. This consists of four bulk phases surrounded by a fifth phase, see Figure 9. The initial mesh has over half a million
295 nodes and $\varepsilon = 0.04$. We see the evolution into bulk regions with spherical like minimal surfaces in contact with the fifth phase. Moreover, the central region shifts, in a similar way to the two dimensional problem, to remove any quadruple junctions. Figure 10 shows the iteration counts for the solver and inactive

set size for the simulation.

300 5. Conclusions

In this work we have presented a robust practical preconditioner for systems of multiphase Allen-Cahn variational inequalities. As mentioned earlier, see Remark 4.1, the need for a reliable and efficient solver is crucial when using iterative methods to solve the linear systems arising in the PDAS algorithm, where solve tolerances have to be small. Firstly, when exactly solving the matrices in the preconditioning system, in the case of two phases, it was shown, in Theorem 3.1, that GMRES will converge within three iterations. Secondly, in the case of multiple phases, it was shown experimentally, that the use of the inexact preconditioner $P_{3,AMG}$ leads to low GMRES iteration counts on fine meshes. Finally, given the standard blocks used in this solver, i.e., Multigrid, GMRES and simple smoothers, the proposed approach may immediately be applied in most of the software packages used to solve multiphase variational inequalities.

315 Acknowledgements

VS would like to thank the Isaac Newton Institute for Mathematical Sciences for support and hospitality during the programme *Geometry, compatibility and structure preservation in computational differential equations* when work on this paper was undertaken. This work was supported by: EPSRC grant number EP/R014604/1.

ElliottLuckhaus

- [1] C. M. Elliott, S. Luckhaus, A generalised diffusion equation for phase separation of a multi-component mixture with interfacial free energy, IMA Preprint series 887.

AllenCahn1979

- [2] S. M. Allen, J. W. Cahn, A microscopic theory for antiphase motion and its application to antiphase domain coarsening., Acta Metall. Mater. 27 (1979) 1085–1095.

BR [3] L. Bronsard, F. Reitich, On three-phase boundary motion and the singular limit of a vector-valued Ginzburg-Landau equation, Arch. Rat. Mech. Anal. 124 (1993) 355–379.

GNS1993³³⁰ [4] H. Garcke, B. Nestler, B. Stoth, A multi phase field concept: numerical simulations of moving phase boundaries and multiple junctions, SIAM J. Appl. Math. 60 (1999) 295–315.

TK2009 [5] D. Kay, A. Tomasi, Color image segmentation by the vector-valued Allen–Cahn phase-field model: a multigrid solution, IEEE Trans. Image Processing 18 (2009) 2330–2339.

335

Deckelnick2005 [6] K. Deckelnick, C.M. Elliott, and G. Dziuk, Computation of geometric partial differential equations and mean curvature flow, Acta Numerica 14 (2005) 139–232.

DES [7] K. Deckelnick, C. Elliott, V. Styles, Double obstacle phase field approach to an inverse problem for a discontinuous diffusion coefficient, Inverse Problems 32.

340

DorVil08 [8] O. Dorn, R. Villegas, History matching of petroleum reservoirs using a level set technique, Inverse Problems 24 (3) (2008) 035015.

IglMcL11 [9] M. A. Iglesias, D. McLaughlin, Level-set techniques for facies identification in reservoir modeling, Inverse Problems 27 (3) (2011) 035008.

345

IglLinStu14 [10] M. A. Iglesias, K. Lin, A. M. Stuart, Well-posed Bayesian geometric inverse problems arising in subsurface flow, arXiv preprint arXiv:1401.5571.

CheIsaNew99 [11] M. Cheney, D. Isaacson, J. C. Newell, Electrical impedance tomography, SIAM review 41 (1) (1999) 85–101.

DorMilRap03³⁵⁰ [12] O. Dorn, E. L. Miller, C. M. Rappaport, A shape reconstruction method for electromagnetic tomography using adjoint fields and level sets, Inverse problems 16 (5) (2000) 1119.

BoyAdlLio12

- [13] A. Boyle, A. Adler, W. R. B. Lionheart, Shape deformation in two-dimensional electrical impedance tomography, *Medical Imaging, IEEE Transactions on* 31 (12) (2012) 2185–2193.

355

WZ

- [14] M. Wang, S. Zhou, 3d multi-material structural topology optimization with the generalized Cahn–Hilliard equations, *Comput. Model. Eng. Sci* 16 (2007) 89–111.

BFGS

- [15] L. Blank, M. H. Farshaf-Shaker, G. H., V. Styles, Relating phase field and sharp interface approaches to structural topology optimisation, *ESAIM: COCV* 20 (2014) 1025–1058.

360

KK2

- [16] R. Kornhuber, R. Krause, On multigrid methods for vector-valued Allen–Cahn equations, in: H. et al. (Ed.), *Domain Decomposition Methods in Science and Engineering*, UNAM, Mexico City, Mexico, 2003, pp. 307–314.

KK2006

365

- [17] R. Kornhuber, R. Krause, Robust multigrid methods for vector-valued Allen–Cahn equations with logarithmic free energy, *Comput. Vis. Sci.* 9 (2006) 103–116.

GNSW

- [18] H. Garcke, B. Nestler, B. Stinner, F. Wendler, Allen–Cahn systems with volume constraints, *M³AS: Math. Models Methods in Appl. Sci.* 18 (2008) 1347–1381.

370

BlankGarckeSarbuStyles2013

- [19] L. Blank, H. Garcke, L. Sarbu, V. Styles, Nonlocal Allen–Cahn systems: analysis and a primal–dual active set method, *IMA Journal of Numerical Analysis* 33 (2013) 1126–1155.

BIK

- [20] M. Bergounioux, K. Ito, K. Kunisch, Primal-dual active set strategy for constrained optimal control problems, *SIAM J. Control Optim.* 37 (1999) 1176–1194.

375

HIK

- [21] M. Hintermüller, K. Ito, K. Kunisch, The primal-dual active set strategy as a semismooth Newton method, *SIAM J. Optim.* 13 (2002) 865–888.

blanksarbustoll12012

380

- [22] L. Blank, L. Sarbu, M. Stoll, Preconditioning for Allen–Cahn variational inequalities with non-local constraints, *Journal of Computational Physics* 231 (2012) 5406–5420.

GKCH

- [23] C. Gräser, R. Kornhuber, Nonsmooth Schur–Newton methods for multi-component Cahn–Hilliard systems, *IMA J. Num. Anal.* 35 (2014) 652–679.

murphy2000note

385

- [24] M. F. Murphy, G. H. Golub, A. J. Wathen, Note on preconditioning for indefinite linear systems, *SIAM Journal on Scientific Computing* 21 (2000) 1969–1972.

kay2002preconditioner

- [25] D. Kay, D. Loghin, A. Wathen, A preconditioner for the steady-state Navier–Stokes equations, *SIAM Journal on Scientific Computing* 24 (2002) 237–256.

ElmanSilvesterwathenbook

390

- [26] D. Silvester, H. Elman, A. Wathen, *Finite Elements and Fast Iterative Solvers: With Applications in Incompressible Fluid Dynamics*, Oxford University Press, New York, 2005.

saadi1996iterative

- [27] Y. Saad, *Iterative Methods for Sparse Linear Systems*, 2nd Edition, SIAM, Philadelphia, 1996.

Blank_scalar_nonlocal

395

- [28] L. Blank, H. Garcke, L. Sarbu, V. Styles, Primal–dual active set methods for Allen–Cahn variational inequalities with nonlocal constraints, *Numerical methods in partial differential equations* 3 (2013) 999–1030.

hackbuschbook

- [29] W. Hackbusch, *Multi-grid Methods and Applications*, 2nd Edition, Springer, 2003.

stuben2001

400

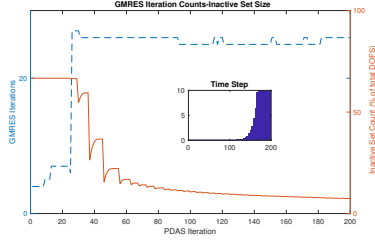
- [30] K. Stüben, A review of algebraic multigrid, *Journal of Computational and Applied Mathematics* 128 (2001) 281–309.

elman99

- [31] H. C. Elman, Preconditioning for the steady-state Navier–Stokes equations with low viscosity, *SIAM Journal on Scientific Computing* 20 (1999) 1299–1316.

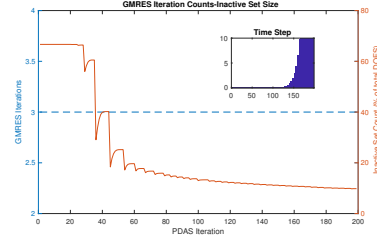
campbell11996₄₀₅

- [32] S. Campbell, C. F. Ipsen, C. T. Kelley, C. D. Meyer, Gmres and the minimal polynomial, BIT Num. Math. 36 (1996) 664–675.



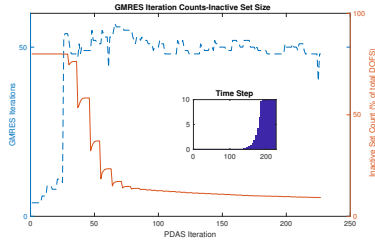
(a) P_1 with $\varepsilon = 0.01$, two phases and Mesh

4



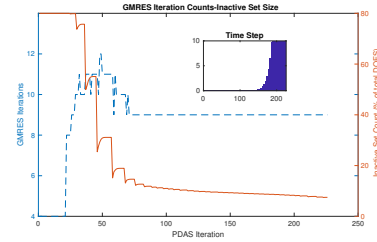
(b) P_3 with $\varepsilon = 0.01$, two phases and Mesh

4

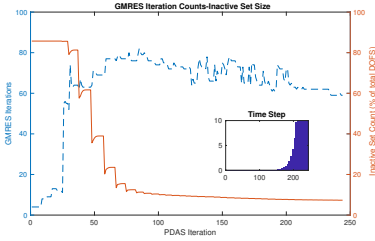


(c) P_1 with $\varepsilon = 0.01$, four phases and Mesh

4

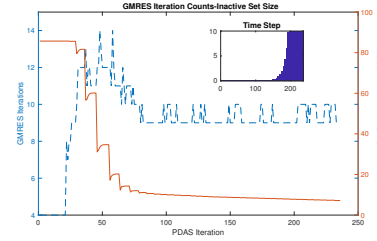


(d) P_3 with $\varepsilon = 0.01$, four phases and Mesh 4



(e) P_1 with $\varepsilon = 0.01$, six phases and Mesh

4

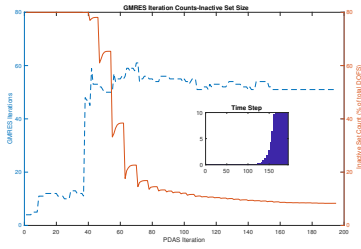


(f) P_3 with $\varepsilon = 0.01$, six phases and Mesh

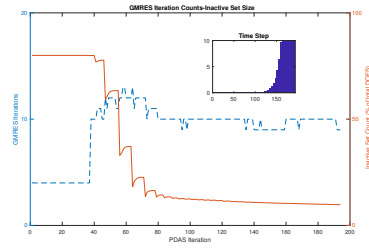
4

fig: Stoll-Kay phase

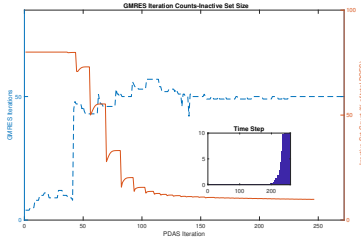
Figure 2: Phase dependence of the exact preconditioners P_1 (left) and P_3 (right).



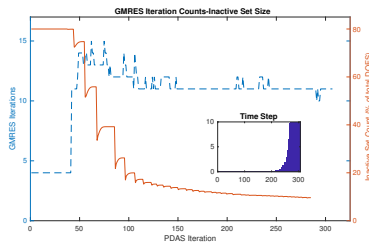
(a) P_1 with $\varepsilon = 0.02$, four phases and Mesh 3



(b) P_3 with $\varepsilon = 0.02$, four phases and Mesh 3



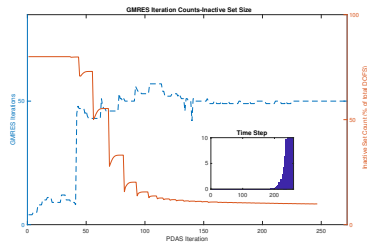
(c) P_1 with $\varepsilon = 0.02$, four phases and Mesh 4



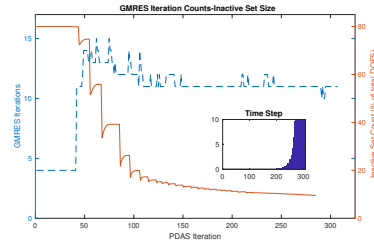
(d) P_3 with $\varepsilon = 0.02$, four phases and Mesh 4

fig: Stoll-Kay mesh

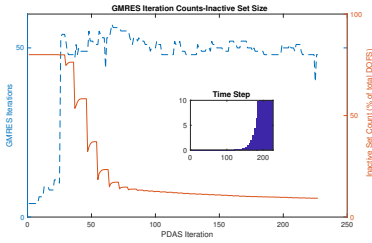
Figure 3: Mesh dependence of the exact preconditioners P_1 (left) and P_3 (right).



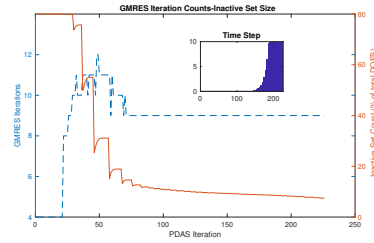
(a) P_1 with $\varepsilon = 0.02$, four phases and Mesh 4



(b) P_3 with $\varepsilon = 0.02$, four phases and Mesh 4



(c) P_1 with $\varepsilon = 0.01$, four phases and Mesh 4



(d) P_3 with $\varepsilon = 0.01$, four phases and Mesh 4

fig: Stoll-Kay epsilon

Figure 4: ε dependence of the exact preconditioners P_1 (left) and P_3 (right).

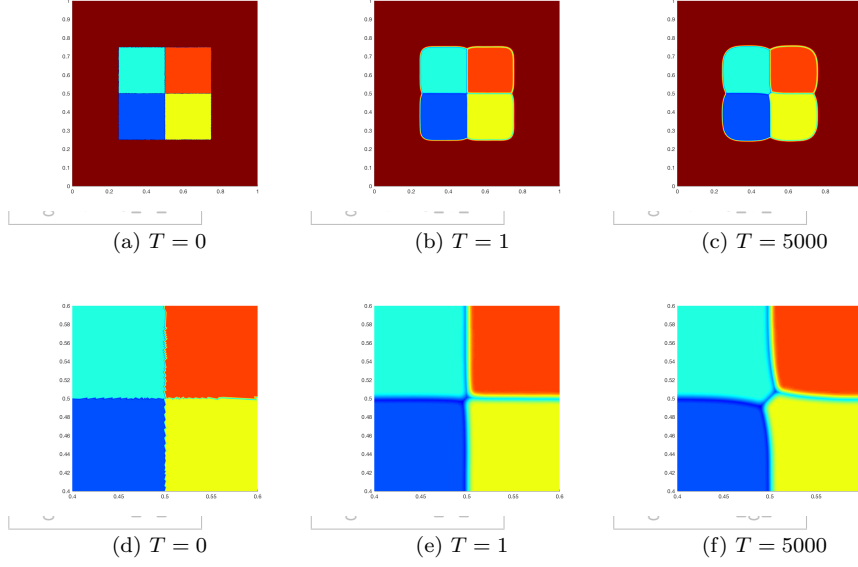


Figure 5: Time evolution of four bulk phases surrounded by a fifth phase, $\varepsilon = 1/200$ and 236868 DOFs for each phase.

fig: 5 phase bulk

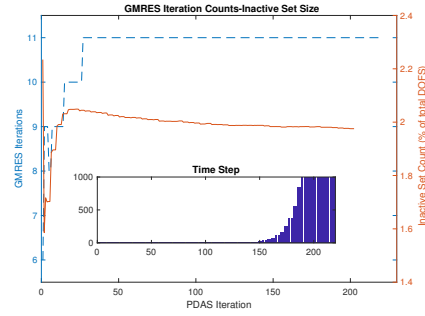


Figure 6: GMRES iterations for the inexact preconditioner $P_{3,AMG}$ and inactive set size, for the simulation presented in Fig. 5 of four bulk phases surrounded by a fifth phase.

fig: 5 bulk GMRES

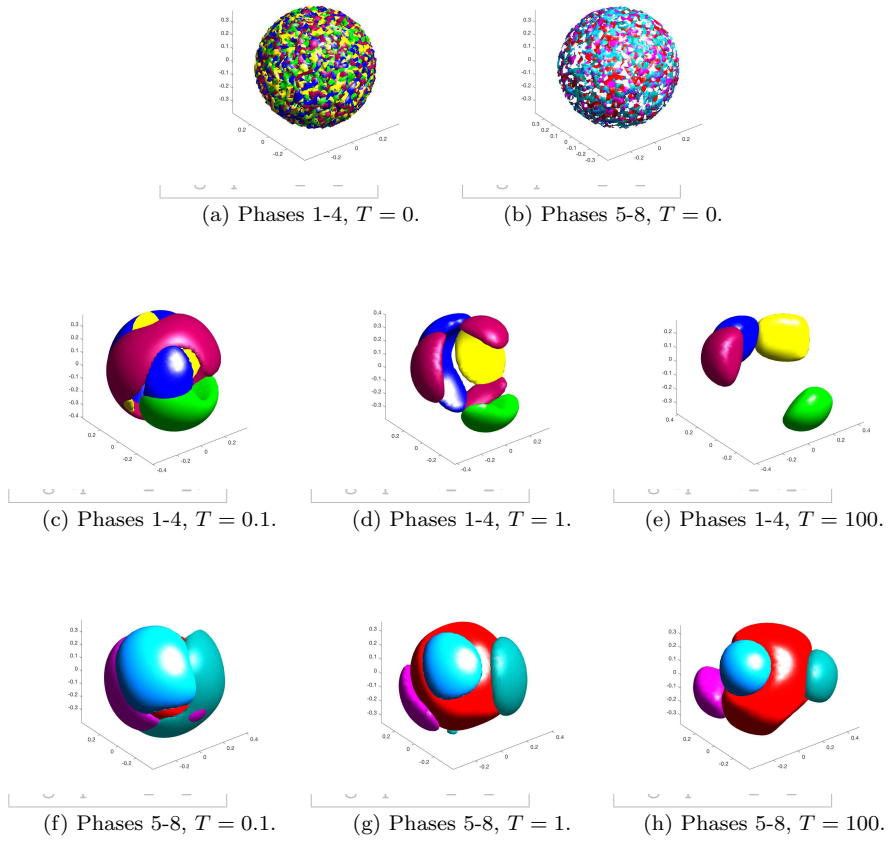


Figure 7: Initial condition is a central sphere containing eight well mixed phases, surrounded by a ninth pure phase.

fig: 9 phase spin 3D

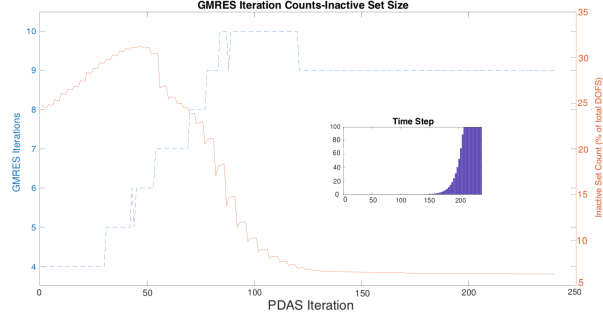


Figure 8: GMRES iterations for the inexact preconditioner $P_{3,AMG}$ and inactive set size, for the simulation presented in Fig. 7 of a well mixed initial condition of nine phases in three space dimensions.

fig: 9 phase spin 3D GMRES

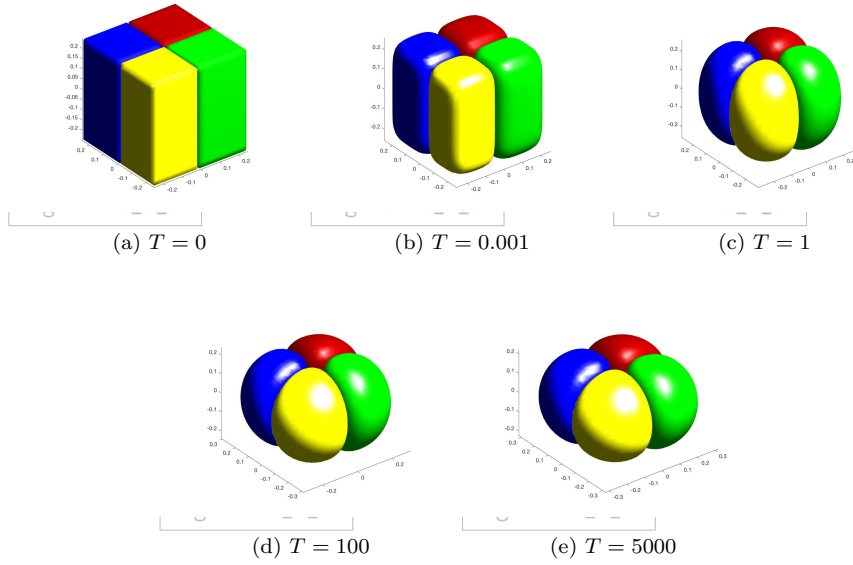


fig: 5 phase bulk 3D

Figure 9: Time evolution of four bulk phases surrounded by a fifth phase.

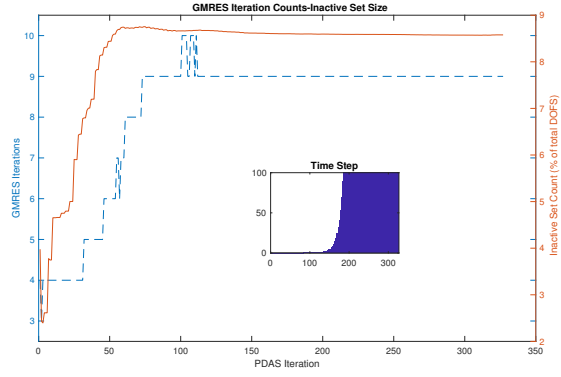


Figure 10: GMRES iterations for the inexact preconditioner $P_{3,AMG}$ and inactive set size, for the simulation presented in Fig. 9 of four bulk phases surrounded by a fifth phase.

fig: 6 phase bulk 3D